



# Cisplatin crosslinked pH-sensitive nanoparticles for efficient delivery of doxorubicin



Mingqiang Li<sup>a,e</sup>, Zhaohui Tang<sup>a</sup>, Shixian Lv<sup>a,e</sup>, Wantong Song<sup>a</sup>, Hua Hong<sup>d</sup>, Xiabin Jing<sup>c</sup>, Yuanyuan Zhang<sup>b,\*\*</sup>, Xuesi Chen<sup>a,\*</sup>

<sup>a</sup> Key Laboratory of Polymer Ecomaterials, Changchun Institute of Applied Chemistry, Chinese Academy of Sciences, Changchun 130022, PR China

<sup>b</sup> Wake Forest Institute for Regenerative Medicine, Wake Forest School of Medicine, Medical Center Boulevard, Winston-Salem, NC 27157, USA

<sup>c</sup> State Key Laboratory of Polymer Physics and Chemistry, Changchun Institute of Applied Chemistry, Chinese Academy of Sciences, Changchun 130022, PR China

<sup>d</sup> Laboratory Animal Center, Jilin University, Changchun 130012, PR China

<sup>e</sup> University of Chinese Academy of Sciences, Beijing 100049, PR China

## ARTICLE INFO

### Article history:

Received 20 December 2013

Accepted 8 January 2014

Available online 1 February 2014

### Keywords:

Drug delivery

Chemotherapy

Crosslinking

Nanoparticle

Polysaccharide

Controlled drug release

## ABSTRACT

pH responsive cisplatin prodrug crosslinked polysaccharide-based nanoparticles were developed from succinic acid decorated dextran (Dex-SA) for active loading and triggered intracellular release of doxorubicin (DOX). Nanoparticles with uniform size were formed spontaneously in aqueous medium *via* electrostatic interaction between anionic Dex-SA and cationic DOX, and subsequently transformed into crosslinked nanoparticles (CL-Nanoparticles) *in situ* by readily crosslinking the micelles *via* chelate interactions between the ionic polymeric carrier and the platinum (II) antitumor drug. This strategy eliminated the need of organic solvents and sophisticated processes in the drug loading procedure. The *in vitro* release studies showed that DOX was released from the CL-Nanoparticles in a controlled and pH-dependent manner. Furthermore, the pharmacokinetics and biodistribution investigations indicated that, as compared to the non-crosslinked nanoparticles (NCL-Nanoparticles) and free DOX, the CL-Nanoparticles significantly prolonged the blood circulation time of drug, decreased accumulation in the normal tissues and enriched drug into the tumors. As a consequence, the DOX-loaded CL-Nanoparticles exhibited enhanced therapeutic efficacy in tumor-bearing mice compared with the NCL-Nanoparticles and free DOX, which were further confirmed by the histological and immunohistochemical analyses. These cisplatin prodrug crosslinked polysaccharide nanoparticles proved to be a promising nanomedicine drug delivery system for tumor-targeted delivery of DOX.

© 2014 Elsevier Ltd. All rights reserved.

## 1. Introduction

Doxorubicin hydrochloride, an amphiphilic anticancer drug, is a leading clinically-used anticancer drug due to its potency and a broad spectrum of activity against diverse cancer types (e.g., breast, lung, prostate, brain, cervix, bone, and bladder cancers) [1]. Current drug delivery systems involving doxorubicin (DOX) are mostly based on hydrophobic interaction between the drug and hydrophobic moieties of the drug carrier. As a general rule, DOX hydrochloride was neutralized by excess triethylamine to remove the hydrochloride and DOX becomes hydrophobic in organic solvents (dimethyl formamide or dimethylsulfoxide) [2–4]. Nevertheless,

the hydrophobization treatment on the amphiphilic DOX hydrochloride significantly reduces its anticancer activity [4]. The second most potent anticancer drug is cisplatin that has also been widely used for many malignancies, such as ovarian, head and neck, gastrointestinal, testicular, bladder, and lung cancers [5]. Combination chemotherapy (using two or more drugs proven effective against a tumor type) often brings about advantage such as enhancing the overall cytotoxicity of each drug against cancer cells at reduced doses, maximizing therapeutic efficacy against individual drug targets, and overcoming drug resistance [6]. For this specific reason, Nguyen's group developed a single polymer-caged nanobin with both DOX and cisplatin, which yielded strong synergy in the efficacy of these agents [7]. Recently, Yang and co-workers demonstrated that the presence of the carboxyl groups in micelles significantly increased loading capacity of DOX due to ionic interactions between the carboxyl group in the micelle and amine group in the drug [8–10]. Meanwhile, our previous study also

\* Corresponding author. Tel./fax: +86 431 85262112.

\*\* Corresponding author. Tel.: +1 336 713 1189; fax: +1 336 713 7290.

E-mail addresses: [y Zhang@wakehealth.edu](mailto:y Zhang@wakehealth.edu) (Y. Zhang), [xschen@ciac.ac.cn](mailto:xschen@ciac.ac.cn) (X. Chen).

proved that anionic PEGylated polypeptide could load relatively large amount of cisplatin or cationic DOX for effective treatment of lung cancer and hepatoma [11–14].

Anticancer drugs are often delivered by utilization of polymeric micelles, however the extracellular stability versus intracellular drug release dilemma via this delivery system remains a challenge [15,16]. One potential solution is the use of reversible crosslinked micelles, which can simultaneously enhance their stability outside the cells, while efficiently breaking their crosslink inside cells in response to the appropriate stimuli, and thus releasing the payload [17]. Progress has been achieved in developing stimuli-responsive crosslinked micelles, including enzymatically cleavable [18–20], pH-cleavable [21], disulfide or diselenide bond-containing [22], and hydrolysable ester-bond-containing [23] micellar nanoparticles. Even more promising are micellar nanoparticles which are responsive to multiple stimuli as reported recently for the precise spatiotemporal drug release in the complex *in vivo* microenvironment, showing the benefits of high drug loading efficiency, superior stability against dilution, prolonged circulation time, and enhanced drug accumulation at the tumor site [16,24,25]. Although great progress has been achieved in this field, effective methods for facile synthesis of the simple yet efficient stimuli-responsive crosslinked micelles are still much in demand. To the best of our knowledge, the application of cisplatin as the crosslinker for efficient doxorubicin hydrochloride delivery has not been studied yet.

In the present study, taking the advantage of cisplatin prodrug (an inactive substance that is converted to cisplatin within the body by the action of chloridion or acidic species) as the crosslinker, we explore the potential of carboxylic ligands functionalized dextran as the carrier for DOX delivery. Towards this aim, we firstly synthesized the carboxyl groups modified polysaccharide dextran-succinic acid (Dex-SA), which was then used to adsorb doxorubicin hydrochloride electrostatically in aqueous solution and self-assembled into polymeric micelles with uniform size. Subsequently, the crosslinked nanoparticles (CL-Nanoparticles, Dex-SA-DOX-CISPLATIN) were synthesized *in situ* by crosslinking the micelles via chelate interactions between the ionic polymeric carrier and the platinum (II) antitumor drug. It is of note that a small amount of cisplatin could effectively stabilize the nanoparticles, and the drug release kinetics could be readily regulated by the crosslinking degree of the DOX-loaded nanoparticles. The effects of crosslinking were studied by comparing the physicochemical properties, the drug release kinetics, cellular uptake, *in vitro* cytotoxicity, pharmacokinetics, tolerability, and tissue distribution, as well as the *in vivo* antitumor efficacy.

## 2. Materials and methods

### 2.1. Materials

Dextran (Dex, 40 kDa) was purchased from Fluka and used without further purification. Succinic anhydride was obtained from Sinopharm Chemical Reagent Co., Ltd. Doxorubicin hydrochloride (Beijing Huafeng United Technology Corporation), cisplatin (Shandong Boyuan Pharmaceutical Co., Ltd.), 4-dimethylaminopyridine (DMAP, Alfa Aesar), 3-(4,5-Dimethyl-thiazol-2-yl)-2,5-diphenyl tetrazolium bromide (MTT, Sigma) and 4',6-diamidino-2-phenylindole dihydrochloride (DAPI, Sigma) were used as received. Dimethyl sulfoxide (DMSO) was stored over calcium hydride (CaH<sub>2</sub>) and purified by vacuum distillation with CaH<sub>2</sub>. Purified deionized water was prepared by the Milli-Q plus system (Millipore Co., Billerica, MA, USA).

### 2.2. Characterization

<sup>1</sup>H and <sup>13</sup>C NMR spectra were recorded on a Bruker AV 400 NMR spectrometer in DMSO-*d*<sub>6</sub>. Fourier transform infrared (FT-IR) spectra were recorded on a Bio-Rad Win-IR instrument using KBr method. GPC analyses of Dex and Dex-SA were conducted on a Waters 2414 system equipped with Ultrahydrogel™ linear column and a Waters 2414 refractive index detector (eluent: 0.1 M phosphate buffer, pH 7.4; flow rate: 0.5 mL min<sup>-1</sup>; temperature: 35 °C; standard: poly(ethylene glycol)). Zeta potentials (ζ-potential) of the samples were measured by Zeta Potential/BI-90Plus

particle size analyzer (Brookhaven Instruments Corporation, USA). Dynamic laser scattering (DLS) measurement was performed on a WyattQELS instrument with a vertically polarized He–Ne laser (DAWN EOS, Wyatt Technology, USA). The scattering angle was fixed at 90°. Inductively coupled plasma optical emission spectrometer (ICP-OES, iCAP 6300, ThermoScientific, USA) and inductively coupled plasma mass spectrometer (ICP-MS, Xseries II, ThermoScientific, USA) were used for quantitative determination of platinum. Transmission electron microscopy (TEM) measurement was performed on a JEOL JEM-1011 transmission electron microscope with an accelerating voltage of 100 KV.

### 2.3. Synthesis of Dex-SA

Dextran (5.002 g, 30.750 mmol AHG) was dissolved in 40 mL of dry DMSO and introduced into a flame-dried flask, followed by addition of 4-(dimethylamino) pyridine (1.878 g, 15.375 mmol) solution in DMSO (5 mL) and succinic anhydride (1.538 g, 15.375 mmol) in DMSO (5 mL), respectively. The reaction was performed at 30 °C for 48 h under nitrogen. The product was isolated by precipitation in cold ethanol, washed several times with ethanol, and dried under vacuum. The resulting white powder was then dissolved in deionized water, dialyzed against phosphate buffer (PB, 0.01 M, pH 7.0) and deionized water for 72 h to remove the excess reactants. The final product was obtained as a white powder after lyophilization of the dialyzed solution.

### 2.4. Preparation of the DOX-loaded nanoparticles

Dex-SA lyophilized powder was dissolved in deionized water and stirred for 10 min, and then its pH was adjusted to 7.4 with a few drops of 0.05 M NaOH. An aqueous solution of doxorubicin hydrochloride was added dropwise into the polymer solution and the mixture solution was vigorously stirred overnight in the dark. Subsequently, a predetermined amount of cisplatin was added into the above mixture and the reaction was continued at 37 °C for 72 h. Excess drug was removed by dialysis (MWCO 3500) against deionized water for 24 h and followed by lyophilization in the dark. The drug loading content (DLC) and drug loading efficiency (DLE) of DOX and cisplatin was determined by using UV–vis spectrometer and ICP-OES. DLC and DLE were calculated according to the following formula:

$$\text{DLC}(\text{wt.}\%) = (\text{weight of loaded drug} / \text{weight of drug} - \text{loaded nanoparticles}) \times 100\%$$

$$\text{DLE}(\text{wt.}\%) = (\text{weight of loaded drug} / \text{weight of feeding drug}) \times 100\%$$

### 2.5. *In vitro* release of DOX

To determine the release profiles of DOX, the weighed freeze-dried DOX-loaded nanoparticles powder was suspended in 10 mL of release medium and transferred into a dialysis bag (MWCO 3500 Da). The release experiment was initiated by placing the end-sealed dialysis bag into 40 mL of release medium at 37 °C with constant shaking. At selected time intervals, 3 mL of release media was taken out and replenished with an equal volume of fresh media. The amount of DOX released was determined using UV–vis spectrometer at 480 nm.

### 2.6. Cell cultures

The human lung carcinoma (A549) cells were cultured at 37 °C in a 5% CO<sub>2</sub> atmosphere in Dulbecco's modified Eagle's medium (DMEM, Gibco) supplemented with 10% fetal bovine serum (FBS), penicillin (50 U mL<sup>-1</sup>) and streptomycin (50 U mL<sup>-1</sup>).

### 2.7. Confocal laser scanning microscopy

The cellular uptake and intracellular release behaviors of the NCL-Nanoparticles and CL-Nanoparticles were determined by confocal laser scanning microscopy toward A549 cells. The cells were seeded on the coverslip in 6-well plates with a density of  $1 \times 10^5$  cells per well in 2 mL of DMEM and cultured for 24 h, and then the original medium was replaced with free DOX, NCL-Nanoparticles and CL-Nanoparticles (at a final DOX concentration of 5 mg L<sup>-1</sup>) containing DMEM. After 1 h and 3 h incubation, the cells were washed and fixed with 4% formaldehyde for 20 min at room temperature, and the cell nuclei were stained with DAPI. The cellular localization was visualized under a laser scanning confocal microscope (Carl Zeiss, LSM 700).

### 2.8. Flow cytometry

A549 cells were seeded in 6-well plates with a density of  $2 \times 10^5$  cells per well in 2 mL of DMEM and incubated for 24 h, and then the original medium was replaced with free DOX, NCL-Nanoparticles and CL-Nanoparticles (at a final DOX concentration of 5 mg L<sup>-1</sup>) containing DMEM. The cells were incubated for 1 h and 3 h at 37 °C, and then washed three times with phosphate buffered saline (PBS). The harvested cells were suspended in PBS and centrifuged at 1000 rpm for 5 min at 4 °C. The supernatants were discarded and the cells were washed with PBS to remove the

background fluorescence in the medium. After two cycles of washing and centrifugation, cells were resuspended with 500  $\mu\text{L}$  PBS, and flow cytometry was done using a BD FACSCalibur flow cytometer from BD Biosciences.

### 2.9. Cytotoxicity assay

The cytotoxicities of Dex-SA, free DOX, NCL-Nanoparticles and CL-Nanoparticles were evaluated by MTT assay. The cells were seeded in 96-well plates ( $1 \times 10^4$  cells per well) in 100  $\mu\text{L}$  of DMEM medium and incubated at 37 °C in a 5%  $\text{CO}_2$  atmosphere for 24 h. The culture medium was replaced with 200  $\mu\text{L}$  of fresh medium containing Dex-SA, free DOX, NCL-nanoparticles and CL-nanoparticles. The cells were subjected to MTT assay after being incubated for another 24 h. The absorbance of the solution was measured on a Bio-Rad 680 microplate reader at 490 nm. The relative cell viability was determined by comparing the absorbance at 490 nm with control wells containing only cell culture medium. Data are presented as means  $\pm$  SD ( $n = 6$ ).

### 2.10. Hemolysis assay

Hemolytic activity of Dex-SA was evaluated according to a previous protocol with minor modification [11,26]. Briefly, fresh rabbit blood obtained from the Laboratory Animal Center of Jilin University was diluted by physiological saline, and then red blood cells (RBC) were isolated from serum by centrifugation. After careful wash and dilution, RBC suspension was added to Dex-SA solution at systematically varied concentrations and mixed by vortex, then incubated at 37 °C in a thermostatic water bath for 2 h. PBS and triton X-100 ( $10 \text{ g L}^{-1}$ ), a surfactant known to lyse RBCs, were used as negative and positive controls, respectively. Then, RBCs were centrifuged at 3000 rpm for 10 min and 100  $\mu\text{L}$  of supernatant of each sample was transferred to a 96-well plate. Free hemoglobin in the supernatant was measured with a Bio-Rad 680 microplate reader at 540 nm. The hemolysis ratio (HR) of RBCs was calculated using the following formula:  $\text{hemolysis (\%)} = (A_{\text{sample}} - A_{\text{negative control}}) / (A_{\text{positive control}} - A_{\text{negative control}}) \times 100$ , where  $A_{\text{sample}}$ ,  $A_{\text{negative control}}$  and  $A_{\text{positive control}}$  were denoted as the absorbencies of samples, negative and positive controls, respectively. All hemolysis experiments were carried out in triplicates.

### 2.11. Pharmacokinetics

Wistar rats (240–250 g) were randomly divided into three groups ( $n = 3$ ). Free DOX, NCL-Nanoparticles and CL-Nanoparticles were administered intravenously via tail vein ( $5 \text{ mg kg}^{-1}$  DOX). At defined time periods (2, 10, 20, 40, 60, 120, 180, 240, 360, 480, 600 and 720 min), blood samples were collected from orbital cavity, heparinized, and centrifuged to obtain the plasma. The concentrations of DOX in the above samples were determined by the HPLC methods reported previously with minor modifications [27,28]. Briefly, a 180  $\mu\text{L}$  plasma sample was deproteinized with 600  $\mu\text{L}$  of acetonitrile, 200  $\mu\text{L}$  of methanol and 100  $\mu\text{L}$  of daunorubicin hydrochloride ( $1 \mu\text{g mL}^{-1}$ , internal standard), vortexed for 10 min, and centrifuged at 13,000 rpm for 10 min. Then 800  $\mu\text{L}$  of supernatant was collected and dried under a stream of nitrogen at 35 °C. The dried sample was then dissolved in the mobile phase for HPLC analysis. Waters liquid chromatographic system (Waters e2695 Separations Module, USA) was equipped with a fluorescence detector (Waters 2475 Multi  $\lambda$  Fluorescence Detector, USA) with the excitation and emission wavelengths set at 472 nm and 592 nm, respectively. A Waters Symmetry C18 analytical column (5  $\mu\text{m}$ ,  $4.6 \times 250 \text{ mm}$ ) was used at 35 °C.

### 2.12. Ex vivo DOX fluorescence imaging

The NCL-Nanoparticles, CL-Nanoparticles and free DOX were injected into mice bearing A549 tumor via lateral tail vein ( $5 \text{ mg kg}^{-1}$  on DOX basis). The mice were sacrificed 3, 10 and 24 h post-injection. The tumor and major organs (heart, liver, spleen, lung and kidney) were excised, followed by washing the surface with physiological saline three times for *ex vivo* imaging of DOX fluorescence using the Maestro *in vivo* Imaging System (Cambridge Research & Instrumentation, Inc., USA). The resulting data can be used to identify, separate, and remove the contribution of autofluorescence in analyzed images by the commercial software (Maestro 2.4). The average signals were also quantitatively analyzed using Maestro 2.4 software.

### 2.13. Evaluation of maximum tolerated dose

Male Kunming mice (at 5–6 weeks of age) were used to evaluate the maximum tolerated dose of free DOX, NCL-Nanoparticles and CL-Nanoparticles. All groups ( $n = 3$ ) received a single dose by intravenous injection. Five groups of mice received DOX, NCL-Nanoparticles and CL-Nanoparticles at a dose of 5, 10, 15, 20, and 25  $\text{mg kg}^{-1}$  DOX. The control groups received saline or 400, 600, 800, and 1000  $\text{mg kg}^{-1}$  of Dex-SA. The body weight and physical states of all the mice were monitored for a period of 10 d. The MTD was defined as the allowance of a median body weight loss of 20% and causes neither death due to toxic effects nor remarkable changes in the general signs within 10 d after administration [29].

### 2.14. In vivo antitumor efficiency

Male Balb/C nude mice were obtained from SLRC Laboratory Animal Company (Shanghai, China), and used at 6 weeks of age. All animals received care in compliance with the guidelines outlined in the Guide for the Care and Use of

Laboratory Animals and all procedures were approved by the Animal Care and Use Committee of Jilin University. A human non-small cell lung cancer (NSCLC) xenograft tumor model was generated by subcutaneous injection of A549 cells ( $1.5 \times 10^6$ ) in the right flank of each mouse. When the tumor volume was approximately 50  $\text{mm}^3$ , mice were randomly divided into 8 groups. Animals were treated with PBS, free DOX ( $3.0 \text{ mg kg}^{-1}$ ), free cisplatin ( $0.32 \text{ mg kg}^{-1}$ ), free DOX ( $3.0 \text{ mg kg}^{-1}$ ) plus free cisplatin ( $0.32 \text{ mg kg}^{-1}$ ), Dex-SA-CISPLATIN ( $0.32 \text{ mg kg}^{-1}$  on cisplatin basis), Dex-SA-DOX ( $3.0 \text{ mg kg}^{-1}$  on DOX basis), Dex-SA-DOX ( $3.0 \text{ mg kg}^{-1}$  on DOX basis) plus Dex-SA-CISPLATIN ( $0.32 \text{ mg kg}^{-1}$  on cisplatin basis) and Dex-SA-DOX-CISPLATIN ( $3.0 \text{ mg kg}^{-1}$  on DOX basis and  $0.32 \text{ mg kg}^{-1}$  on cisplatin basis) by intravenous injection on days 0, 4, 8, and 12. The tumor size was measured using vernier calipers, and the tumor volume ( $\text{mm}^3$ ) was calculated using  $V = a \cdot b^2 / 2$ , where  $a$  and  $b$  were the longest and shortest diameter of the tumors. The body weight was measured simultaneously as an indicator of systemic toxicity.

### 2.15. Histological and immunohistochemical analyses

The mice were sacrificed (at day 6 after the last injections) and the tumors and major organs (heart, liver, spleen, lung and kidney) were collected, fixed in 4% PBS buffered paraformaldehyde overnight, and then embedded in paraffin. The paraffin-embedded tumors and organs were cut at 5  $\mu\text{m}$  thickness, and stained with hematoxylin and eosin (H&E) to assess histological alterations by microscope (Nikon TE2000U).

Immunohistochemistry was performed as described previously [16,30]. Rabbit monoclonal primary antibody for cleaved PARP (Abcam, USA) and PV-6000 two-step immunohistochemistry kit (Zhongshan Goldbridge Biotechnology, Beijing, China) were used in this study.

### 2.16. In situ TUNEL assay

Terminal deoxynucleotidyl transferase-mediated deoxyuridine triphosphate nick end labeling (TUNEL) assay was performed using a FragELTM DNA fragment detection kit (colorimetric-TdT Enzyme method) according to the manufacturer's protocol (EMD chemicals Inc, Darmstadt, Germany).

### 2.17. Statistical analysis

All experiments were performed at least three times and expressed as means  $\pm$  SD. Data were analyzed for statistical significance using Student's test.  $p < 0.05$  was considered statistically significant, and  $p < 0.01$  was considered highly significant.

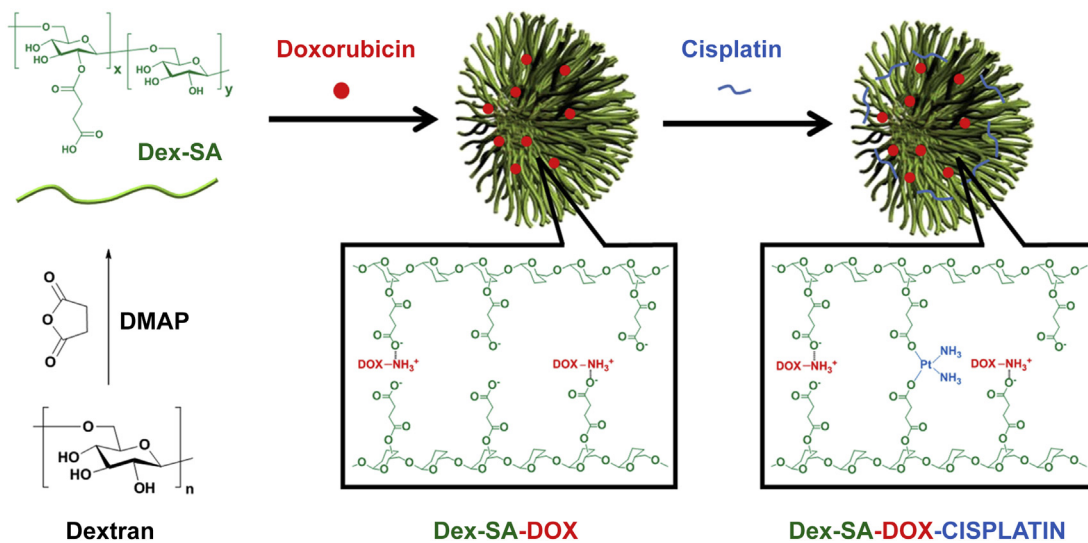
## 3. Results and discussion

### 3.1. Synthesis of Dex-SA

The Dex-SA conjugate was conveniently prepared by treating dextran with succinic anhydride in anhydrous DMSO (Scheme 1). The quantitative  $^1\text{H}$  and  $^{13}\text{C}$  NMR spectra of Dex-SA recorded in DMSO- $d_6$  were displayed in Fig. 1A and B with the relevant signals labeled. The actual degree of substitution (DS, defined as the number of SA units per 100 anhydroglucosidic units) was determined to be 50 by comparing integration areas of peak  $b + c$  ( $-\text{COCH}_2\text{CH}_2\text{CO}-$ , 2C, SA) in the range of 29.8–27.8 ppm with that of peak  $e$  ( $-\text{OCHO}-$ , 1C, Dextran) in the range of 100.1–94.3 ppm. The FT-IR spectrum of Dex-SA (Fig. 1C) clearly revealed the presence of absorbance peak at  $1731 \text{ cm}^{-1}$  characteristic of carboxyl moieties. The GPC trace (Fig. 1D) was monomodal and quite symmetric, revealing the number average molecule weight ( $M_n$ ) of  $3.18 \times 10^4 \text{ g mol}^{-1}$  and polydispersity index (PDI,  $M_w/M_n$ ) of 1.82. In comparison with that of dextran, GPC trace of Dex-SA exhibited a clear shift to the higher  $M_n$  region, indicating that the succinic acid was successfully grafted on to the dextran. A combination of NMR, FT-IR, and GPC verified the successful synthesis of Dex-SA with high purity and moderate polydispersity.

### 3.2. Preparation of the cisplatin crosslinked DOX-loaded Dex-SA nanoparticles

It has been reported that DOX should be administered intravenously as the hydrochloride salt for maximum protection of the drug activity [31]. In the present study, the polysaccharide containing side-chain carboxyl groups provided sites for complexation with



**Scheme 1.** The schematic illustration of the process of preparing Dex-SA, Dex-SA-DOX and Dex-SA-DOX-CISPLATIN.

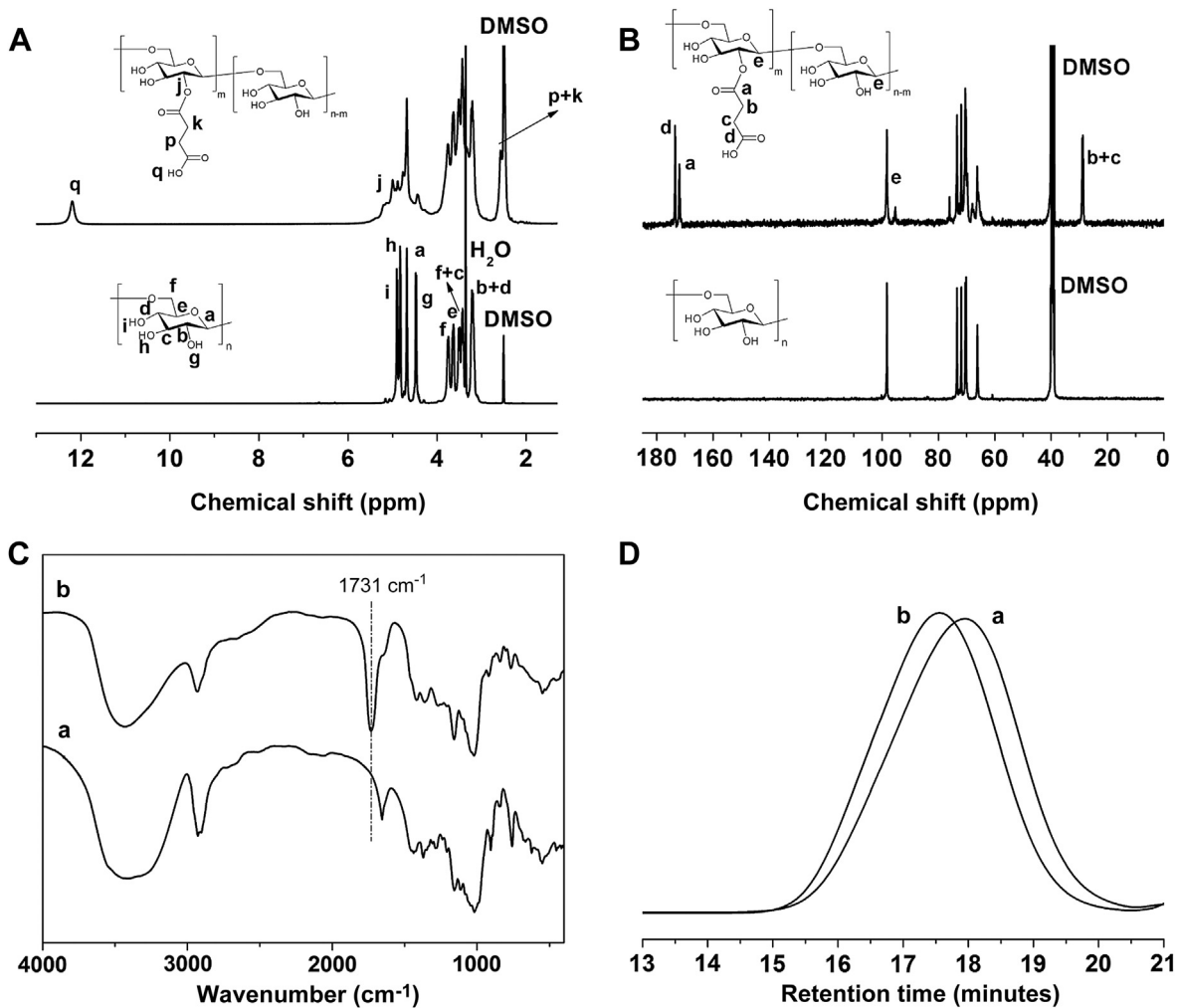


**Fig. 1.** (A) <sup>1</sup>H and (B) <sup>13</sup>C NMR spectra of dextran and Dex-SA in DMSO-*d*<sub>6</sub>; (C) FT-IR spectra obtained for (a) dextran and (b) Dex-SA; and (D) GPC traces recorded for (a) dextran and (b) Dex-SA.

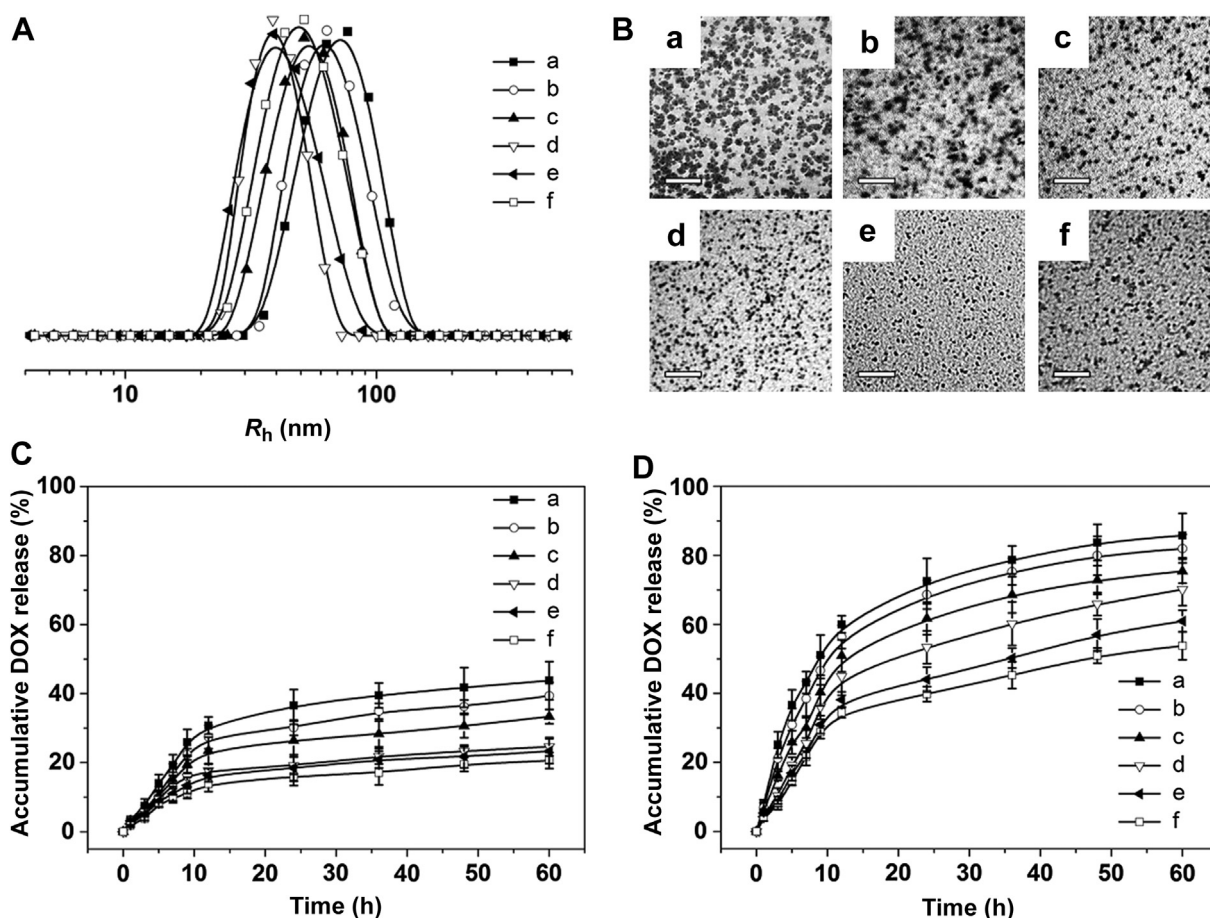


**Fig. 2.** (A) Hydrodynamic radius distribution and (B) morphology of (a) NCL, (b) CL-1, (c) CL-2, (d) CL-3, (e) CL-4 and (f) CL-5 in aqueous solution as determined by DLS and TEM (scale bars: 500 nm); (C and D) Time- and pH-dependent DOX release profiles of (a) NCL, (b) CL-1, (c) CL-2, (d) CL-3, (e) CL-4 and (f) CL-5 in PBS at (C) pH 7.4 and (D) 5.5.

DOX in the active form and cisplatin *via* electrostatic and chelate interactions, respectively. As we know, the usage of organic solvents in pharmaceutical formulations was rarely desirable owing to their potential deleterious effects and the regulatory requirement to quantify residual levels of the harmful organic solvents. A significant advantage of our approach is that the drug loading procedure can be carried out with efficiency in aqueous medium without the use of toxic reagents or organic solvents, thus representing a green chemistry approach. The preparation strategy for the cisplatin crosslinked DOX-loaded Dex-SA nanoparticles (Dex-SA-DOX-CISPLATIN) was shown in Scheme 1. Firstly, DOX loading was performed by incubating the carboxyl-rich polysaccharide Dex-SA with DOX in aqueous medium below its  $pK_a$  value. Then, the DOX-loaded nanoparticles were crosslinked *in situ* by introducing cisplatin (with various molar ratio of carboxylic groups of Dex-SA to cisplatin from 120 to 10) to the solution. After dialyzing the polymer/drug solution

to remove the unloaded drugs, the drug loaded nanoparticles were lyophilized for long-term storage.

The anionic polysaccharide and cationic DOX readily formed nanosized particles in water. The hydrodynamic sizes (radius), as determined by DLS measurements, of the nanoparticles decreased from 71 to 40 nm as the feeding molar ratio of cisplatin and carboxylic group increased from 0 to 0.05 (Fig. 2A and Table 1). The shrinkage of nanoparticles after cross-linking is similar to what has been reported [22]. When the molar ratio of cisplatin and carboxylic group increased to 0.1, an increased hydrodynamic size could be observed. Further increase of the molar ratios, however, resulted in destabilization and precipitation of the nanoparticles. Thus, as can be seen in Table 1, we were able to obtain stable CL-Nanoparticles with [Cisplatin]/[COOH] molar ratio from 0 to 0.1. Such CL-Nanoparticles could be lyophilized and re-dispersed in the aqueous solution. The changes in the particle sizes upon different

**Table 1**  
Characterization of the DOX-loaded NCL- and CL-nanoparticles.

Entry	Feeding molar ratio of [Cisplatin]/[COOH]	Resultant molar ratio of [Cisplatin]/[COOH]	DLC (%)	DLE (%)	Zeta potential (mV)	$R_h$ (nm)
NCL	0	0	15.1	90.8	$-43.3 \pm 6.6$	$71.3 \pm 26.1$
CL-1	1/120.0	1/143.3	14.1	85.0	$-19.6 \pm 3.9$	$63.7 \pm 19.7$
CL-2	1/80.0	1/95.8	13.9	84.2	$-17.2 \pm 2.4$	$54.2 \pm 12.4$
CL-3	1/40.0	1/49.7	13.4	80.6	$-15.9 \pm 3.8$	$39.5 \pm 11.6$
CL-4	1/20.0	1/25.9	12.7	76.8	$-14.7 \pm 4.1$	$40.1 \pm 14.8$
CL-5	1/10.0	1/12.9	12.2	73.8	$-12.9 \pm 2.1$	$48.3 \pm 20.2$

Abbreviation: DOX, doxorubicin; NCL, non-crosslinked; CL, crosslinked; DLC, drug loading content; DLE, drug loading efficiency.

extents of crosslinking were further verified by TEM (Fig. 2B), which were consistent with the variation trends of the DLS measurements. The smaller size from TEM observations should be due to the dehydration of the DOX-loaded nanoparticles in the TEM sample preparation process and the fact that DLS was sensitive to the interference of large particles [32,33]. Zeta-potential analyses demonstrated that these nanoparticles had negative surface charges ( $-43.3$  to  $-12.9$  mV), indicating good dispersion stability [34], which would also minimize the undesirable rapid elimination of DOX-loaded nanoparticles from the blood circulation, and facilitate their accumulation at the tumor sites [35,36]. Besides, it is worthy of note that the surface charge of the CL-Nanoparticles increased from  $-43.3$  to  $-19.6$  mV with the addition of a small amount of cisplatin, revealing the consumption of the carboxylate groups by cisplatin. However, zeta potential increased much slowly with increasing [Cisplatin]/[COOH] ratio. As expected, the DLC and DLE of the CL-Nanoparticles was decreased after crosslinking, which could be due to steric hindrance to drug binding as a result of nanoparticles shrunk and the consumption of the carboxylate groups by cisplatin.

### 3.3. *In vitro* release of DOX

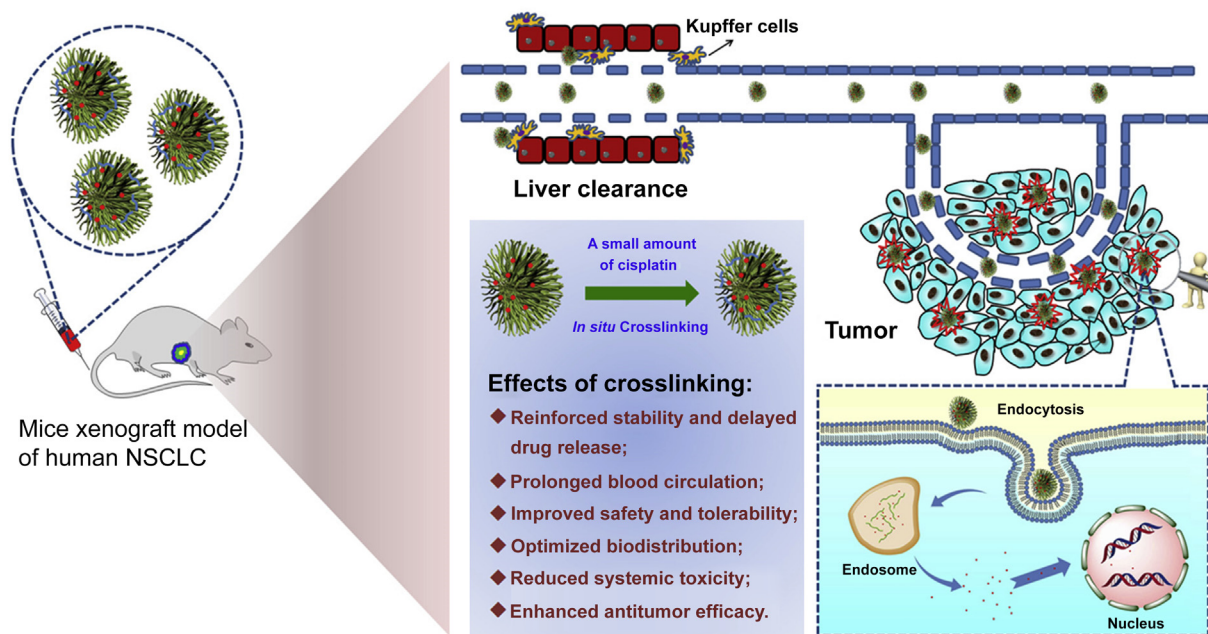
The *in vitro* release of DOX from the NCL and CL-Nanoparticles was carried out at pH 7.4 and 5.5 by dialysis method (Fig. 2C and D). The release profiles showed that no significant initial burst release could be observed and the DOX release rate increased as the pH decreased from 7.4 to 5.5 for both NCL and CL-Nanoparticles. In addition, as compared to the NCL-Nanoparticles, the release of DOX from the CL-Nanoparticles was significantly inhibited at both neutral and acidic pH. Take **CL-3** as an example, at physiological pH, there was approximately 43.8% release for the NCL-Nanoparticles after a 60 h incubation period, while only 24.6% release for the CL-Nanoparticles. Notably, accelerated DOX release at acidic pH was observed for both the NCL- and CL-Nanoparticles, wherein approximately 85.7% and 56.1% of drugs were released in 60 h from NCL- and CL-Nanoparticles, respectively. Drug release under physiological conditions (pH 7.4) was significantly lower than that

under acidic conditions (pH 5.5), which might be attributed to a significant reduction in the ionization degree of SA moieties, resulting in extensive disruption of their electrostatic interactions with DOX [37]. In addition, increased hydrophilicity of DOX in acid condition also resulted in a rapid release of DOX [38]. Such a pH-triggered release behavior of DOX showed great potential in drug delivery for the anti-proliferative effect, due to the release of DOX in cancer cells while limiting its release in blood circulation [16]. Moreover, cisplatin crosslinking could largely enhance micellar stability and might effectively prevent premature drug release following intravenous (i.v.) injection (Scheme 2). The crosslinking degree of the DOX-loaded nanoparticles was correlative to the drug release kinetics, and the release rate was in the following order of **NCL** > **CL-1** > **CL-2** > **CL-3** > **CL-4** > **CL-5** at all the test pH. **CL-3** was chosen for further study because of its appropriate nanoparticle size, which was optimal for tumor targeting by the enhanced permeability and retention (EPR) effect [39].

### 3.4. Intracellular drug delivery

To investigate the cellular internalization and intracellular release of DOX, the DOX-loaded nanoparticles were incubated with A549 cells for 1 h and 3 h at 37 °C. The cells were then observed by confocal laser scanning microscopy (Fig. 3A). DOX fluorescence could be observed in the cells following 1 h incubation with DOX-loaded NCL- and CL-Nanoparticles, which provided clear visual evidence of the cellular internalization of NCL- and CL-Nanoparticles and the release of the loaded DOX molecules. When the incubating time was prolonged to 3 h, DOX was delivered and released into the nuclei of A549 cells, with the DOX fluorescence intensity of CL-Nanoparticles slightly weaker than that of NCL-Nanoparticles. This phenomenon could be explained by the delayed drug release from the CL-Nanoparticles as compared to the NCL-Nanoparticles [40], which was consistent with the data obtained in buffered solutions (Fig. 2C and D).

It should also be noted that stronger DOX fluorescence was observed in cells following incubation with free DOX for 1 and 3 h, compared with the NCL- and CL-Nanoparticles, which could be



**Scheme 2.** The schematic illustration of the blood circulation, tumor accumulation, cellular uptake and pH-responsive intracellular drug release of the CL-Nanoparticles after intravenous injection.

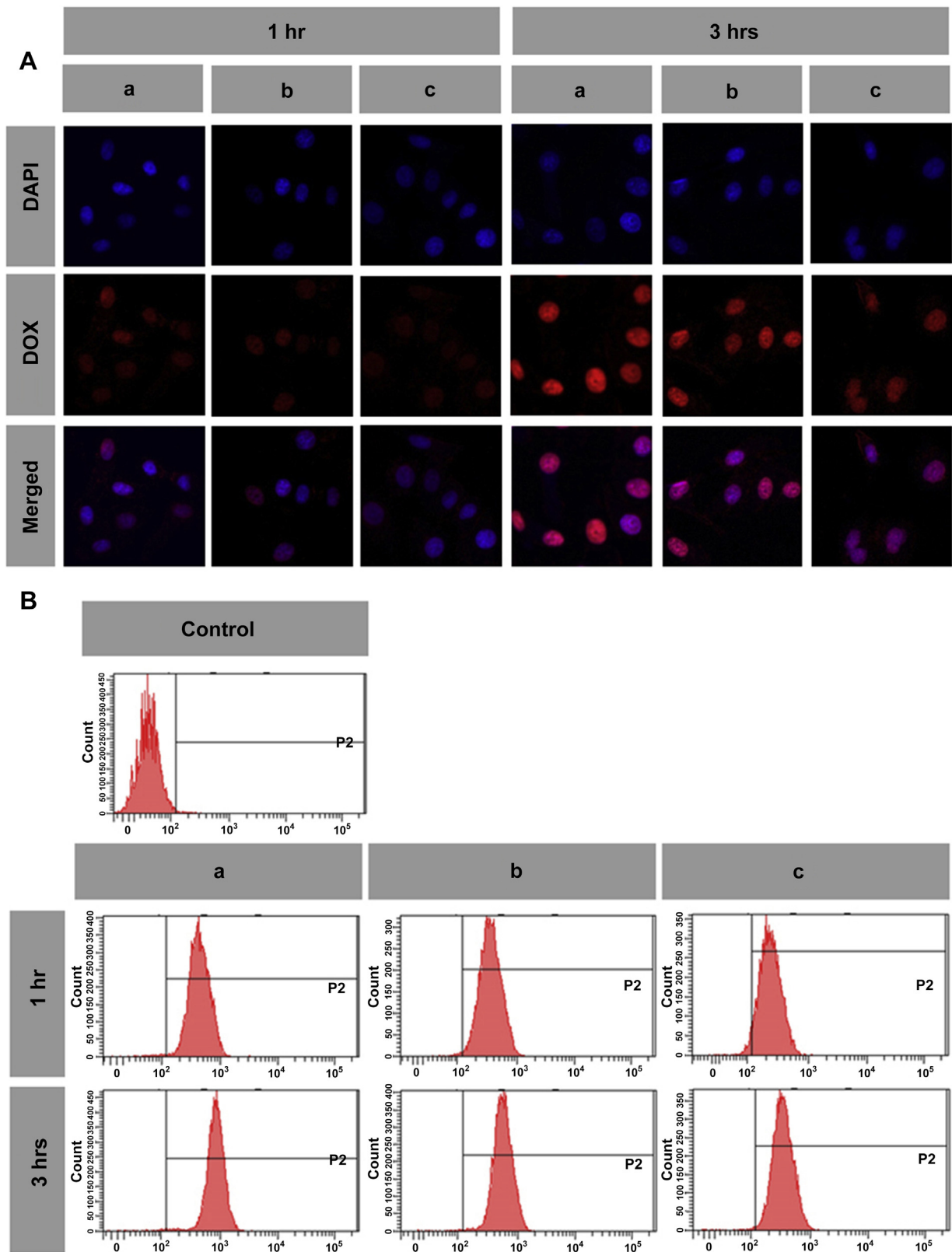


**Fig. 3.** Cellular uptake of (a) free DOX, (b) NCL-Nanoparticles and (c) CL-Nanoparticles after incubation with A549 cells for 1 h and 3 h, observed by (A) confocal laser scanning microscopy and (B) flow cytometric analyses.

attributed to the different cellular internalization mechanisms of the DOX loaded nanoparticles (endocytosis) and free DOX (diffusion) [41]. Additionally, free DOX has been reported to possess stronger fluorescence compared with the DOX in the nanoparticles at the same concentration due to the self-quenching effect of DOX [16,32,42]. Thus, the weaker DOX fluorescence of NCL- and CL-Nanoparticles might be explained by the slightly slower cellular uptake of DOX-loaded nanoparticles and the self-quenching effect of DOX in the NCL- and CL-Nanoparticles [43]. For further confirmation, the cellular uptake of DOX and DOX-loaded NCL- and CL-Nanoparticles into the A549 cells were analyzed using fluorescence-activated flow cytometry (Fig. 3B), and the consistent results were acquired.

### 3.5. *In vitro* cytotoxicity

The biocompatibility studies using A549 cells revealed that Dex-SA was nontoxic up to the highest testing concentration of  $1 \text{ g L}^{-1}$  (Fig. 4A), indicating its excellent biocompatibility. At an equivalent drug concentration, DOX-loaded non-crosslinked nanoparticles revealed a slightly lower cell killing efficiency as compared to free DOX (Fig. 4B), whereas the DOX-loaded crosslinked nanoparticles induced more lower cancer cell killing potency, which agreed well with the *in vitro* drug release behavior and intracellular DOX release observations (Fig. 2C, D and 3A). It was because free DOX could easily diffuse across the cell membrane, while the NCL- and CL-Nanoparticles were internalized through the endocytic pathway, thus resulting in the greater cell uptake and higher cytotoxic efficiency of free DOX [44]. However, for *in vivo* applications, it is unlikely that such a high concentration of free DOX would be present for such a long treatment time [22]. On the other hand, DOX-loaded nanoparticles, especially the crosslinked formulation with long circulating property may facilitate its passive accumulation at tumor tissue via EPR effect [45].

### 3.6. Hemolysis and pharmacokinetics

The application of the vesicular formulations in the pharmaceutical field counts on several aspects including safety, drug loading efficiency and stability. It is necessary to guarantee the blood compatibility of the drug carrier, because it will be finally injected intravenously into blood vessels. In this study, a hemolysis assay was carried out based on the previous report [11,46]. As shown in Fig. 5A, Dex-SA showed negligible hemolysis toxicity ( $\sim 0\%$ ) to RBCs even at the highest polymer concentration of  $5 \text{ g L}^{-1}$ ,

demonstrating the excellent blood compatibility of Dex-SA and the potential application as drug delivery vehicles.

Nanoparticles could be diluted once entering the blood by intravenous administration and this dilution effect may be enlarged when most of the nanoparticles have been distributed into different compartments of the organs (e.g. liver, lung and spleen), leaving only small amounts of nanoparticles circulating in the blood [47,48]. Therefore, the prolonged blood circulation and retardatory blood clearance of nanoparticles is an important issue for effective drug-redistribution to the tumor site [49]. In the present study, plasma pharmacokinetics of free DOX, Dex-SA-DOX and Dex-SA-DOX-CISPLATIN formulations were evaluated with HPLC from plasma after intravenous administration. As shown in Fig. 5B, the disappearance of DOX-loaded NCL-Nanoparticles as well as the free DOX from blood circulation compartment occurred in an exponential manner, whereas plasma DOX concentration of CL-Nanoparticles was the highest at the completion of injection and slowly decreased thereafter, indicating an obvious retardation in clearance from the blood. The blood circulation time of Dex-SA-DOX-CISPLATIN was significantly extended compared to Dex-SA-DOX and free DOX (Fig. 5B), which may promote accumulation in tumor through the EPR effect. The decreased clearance of DOX in plasma in the Dex-SA-DOX-CISPLATIN group compared with the free DOX group might be explained by the *in vitro* delayed drug release (shown in Fig. 2C) and *in vivo* enhanced circulation of nanoparticles based on the slightly negative charged surface of the nano-sized delivery vehicles.

### 3.7. *In vivo* toxicity and tolerability

Despite recent advances in chemotherapeutic agents for cancer, their clinical applications were often limited by systemic toxicity. To determine the toxicity and tolerability of the DOX-loaded NCL- and CL-Nanoparticles, we estimated the MTD by a single i.v. administration to Kunming mice. The weights and survival details of the mice were monitored for 10 days after injection of Dex-SA at doses of 0, 600, 800 and  $1000 \text{ mg kg}^{-1}$ , and free DOX, Dex-SA-DOX and Dex-SA-DOX-CISPLATIN at doses of 5, 10, 15, 20 and  $25 \text{ mg kg}^{-1}$  DOX equivalents (Fig. 6). No morbidity, death or weight loss was observed for Dex-SA at dose up to  $1000 \text{ mg kg}^{-1}$ , indicating its excellent biocompatibility and a potential clinical utility. As expected, a significant loss of body weight was observed at 15, 20 and  $25 \text{ mg kg}^{-1}$  of free DOX, and all the mice in the groups treated with doses of free DOX higher than  $15 \text{ mg kg}^{-1}$  died within 4 days post-injection. In contrast, the DOX-loaded nanoparticles, especially the CL-Nanoparticles could effectively reduce the systemic toxicity

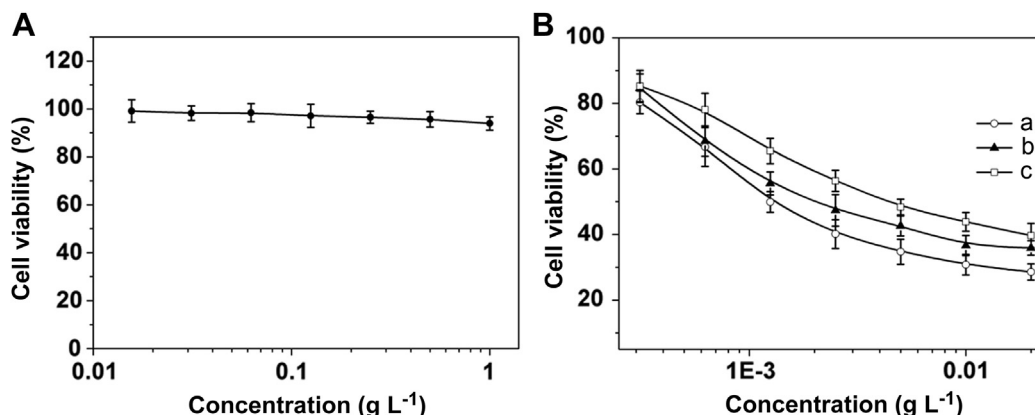
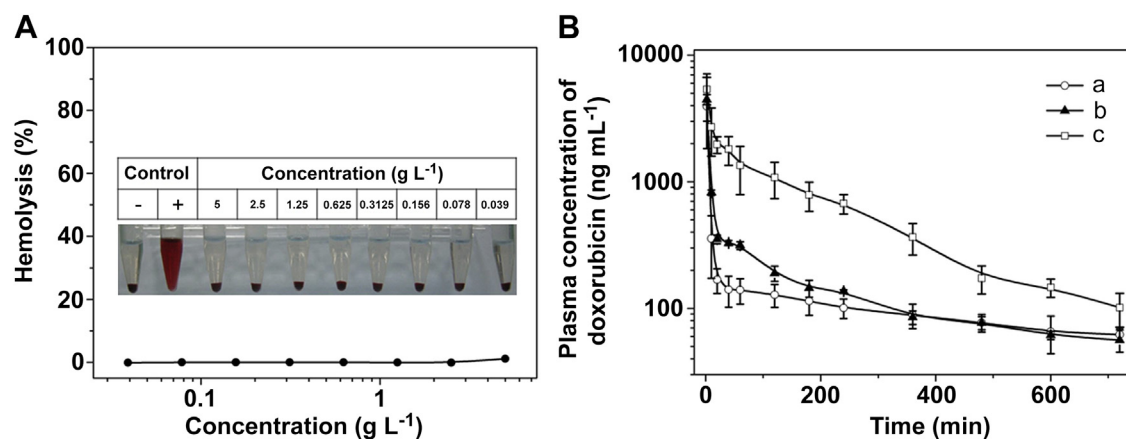


Fig. 4. (A) *In vitro* cytotoxicities of Dex-SA to A549 cells; (B) Cytotoxicities of (a) free DOX, (b) NCL-Nanoparticles and (c) CL-Nanoparticles to A549 cells.



**Fig. 5.** (A) Hemolytic activity of Dex-SA; (B) *In vivo* pharmacokinetics profiles after intravenous injection of (a) free DOX, (b) Dex-SA-DOX and (c) Dex-SA-DOX-CISPLATIN in rats. Data are presented as a mean  $\pm$  standard deviation ( $n = 3$ ).

with a significant prolongation of survival time, less weight loss at all doses and gradual recovery of body weight. The MTD was estimated based on the threshold at which all animals survived and the body weight loss was below 20% [50], and the corresponding MTD of free DOX was determined to be  $5 \text{ mg kg}^{-1}$ , which was in accordance with previous studies [51]. However, DOX-loaded NCL- and CL-Nanoparticles were able to increase the MTD of DOX to 10 and  $15 \text{ mg kg}^{-1}$  (2 and 3 fold of free DOX), respectively. Dose intensification of DOX in a clinical setting is significant as it may allow patients to receive a full dose of chemotherapy without the dose limiting toxicities. This result suggested that the MTD of DOX can be increased through Dex-SA micelle-mediated delivery, and the crosslinked formulation with prolonged drug release could further increase the MTD and reduce systemic toxicity simultaneously.

### 3.8. *Ex vivo* DOX fluorescence imaging

For biodistribution studies, imaging of the isolated solid organs (heart, liver, spleen, lung and kidney) and tumors at 3, 10 and 24 h post-injection were carried out in nude mice bearing A549 tumors, and the fluorescence intensity was semi-quantitatively analyzed (Fig. 7). At 3 h post-injection, liver and kidney showed strong DOX fluorescence for free DOX group, suggesting that drug molecules as foreign bodies were mainly captured and metabolized by liver and kidney [52]. However, compared with free DOX, the fairly weaker fluorescence in kidney for the injection of Dex-SA-DOX and Dex-SA-DOX-CISPLATIN was observed, which could be explained by the significantly improved pharmacokinetics of the nanomedicine formulations. In addition, a favorable biodistribution with increased and decreased accumulation in tumor and the normal tissues (especially for liver and kidney), respectively, for the injection of Dex-SA-DOX-CISPLATIN, could be observed. These results indicated that the CL-Nanoparticles were able to alter the bio-distribution of the drug and provide significant benefits to enhance the tumor accumulation of the DOX and reduce the drug's systemic toxicity.

Notably, a higher intensity of Dex-SA-DOX in the liver was measured as compared to free DOX and Dex-SA-DOX-CISPLATIN, implicating that the liver readily captured DOX-loaded Dex-SA micelles. This is consistent with previous report: undesirable liver uptake was very high for highly positively or negatively charged nanoparticles, which was likely due to active phagocytosis by macrophages (Kupffer cells) in the liver [35]. Consequently, slightly negative charged surface and enhanced micellar stability of DOX-loaded Dex-SA micelles after cisplatin crosslinking appeared to be

particularly significant for blood circulation and tumor accumulation (Scheme 2). The photon numbers per unit area (average signals) shown in Fig. 7B indicated that the CL-Nanoparticles delivered DOX to the tumor with around 1.36 and 1.27-fold higher concentration than DOX and NCL-Nanoparticles groups, respectively. Equally important, the NCL- and CL-Nanoparticles reduced the concentration of DOX in heart by 59% and 63%, and in kidney by 38% and 57%, respectively, as compared to the free DOX. This indicated that the use of Dex-SA micelle or cisplatin crosslinked Dex-SA nanoparticles as a DOX carrier could minimize the possibility of DOX-associated side effects in the heart and kidney, such as cardiomyopathy, congestive heart failure and toxic nephrosis [53]. These data also convincingly demonstrated that the MTD of DOX could be increased through cisplatin crosslinked Dex-SA micelle-mediated delivery. Similar patterns were also been observed at 10 h and 24 h post-injection. Better yet, the DOX-loaded nanoparticles, especially the crosslinked ones increased accumulation in tumor over time, which could contribute to increase the cancer therapy efficiency by EPR effect [54], while free DOX showed nearly invariable fluorescence intensity.

### 3.9. *In vivo* anticancer efficacy

Owing to the enhanced tolerability, prolonged circulation and good tumor localization, the DOX-loaded CL-Nanoparticles might contribute to superior antitumor efficacy without unexpected side effects. To provide *in vivo* evidence for the antitumor potential of Dex-SA-DOX-CISPLATIN, the antitumor efficacy was further investigated on Balb-c/nude mice bearing human lung tumors (A549). The treatments were done by intravenously injecting PBS, free DOX, free cisplatin, free DOX plus free cisplatin, Dex-SA-CISPLATIN, Dex-SA-DOX, Dex-SA-DOX plus Dex-SA-CISPLATIN and Dex-SA-DOX-CISPLATIN, respectively, into tumor-bearing mice.

As shown in Fig. 8A, compared with the control group (treatment with PBS), the tumor growth was effectively inhibited in all the groups treated with free DOX and the DOX-loaded formulations ( $p < 0.001$ ), whereas there was no clear inhibition efficiency on free cisplatin and Dex-SA-CISPLATIN. As compared to Dex-SA-DOX (group f) or free DOX (group b,  $p < 0.01$ , compared with Dex-SA-DOX-CISPLATIN), intravenous injection of Dex-SA-DOX-CISPLATIN (group h) was more efficient in inhibiting tumor growth, indicating that the cisplatin prodrug crosslinked structure was responsible for tumor suppression. Note that the tumor inhibition in group g (the combination of Dex-SA-DOX and Dex-SA-CISPLATIN) was not as effective as group h (Dex-SA-DOX-

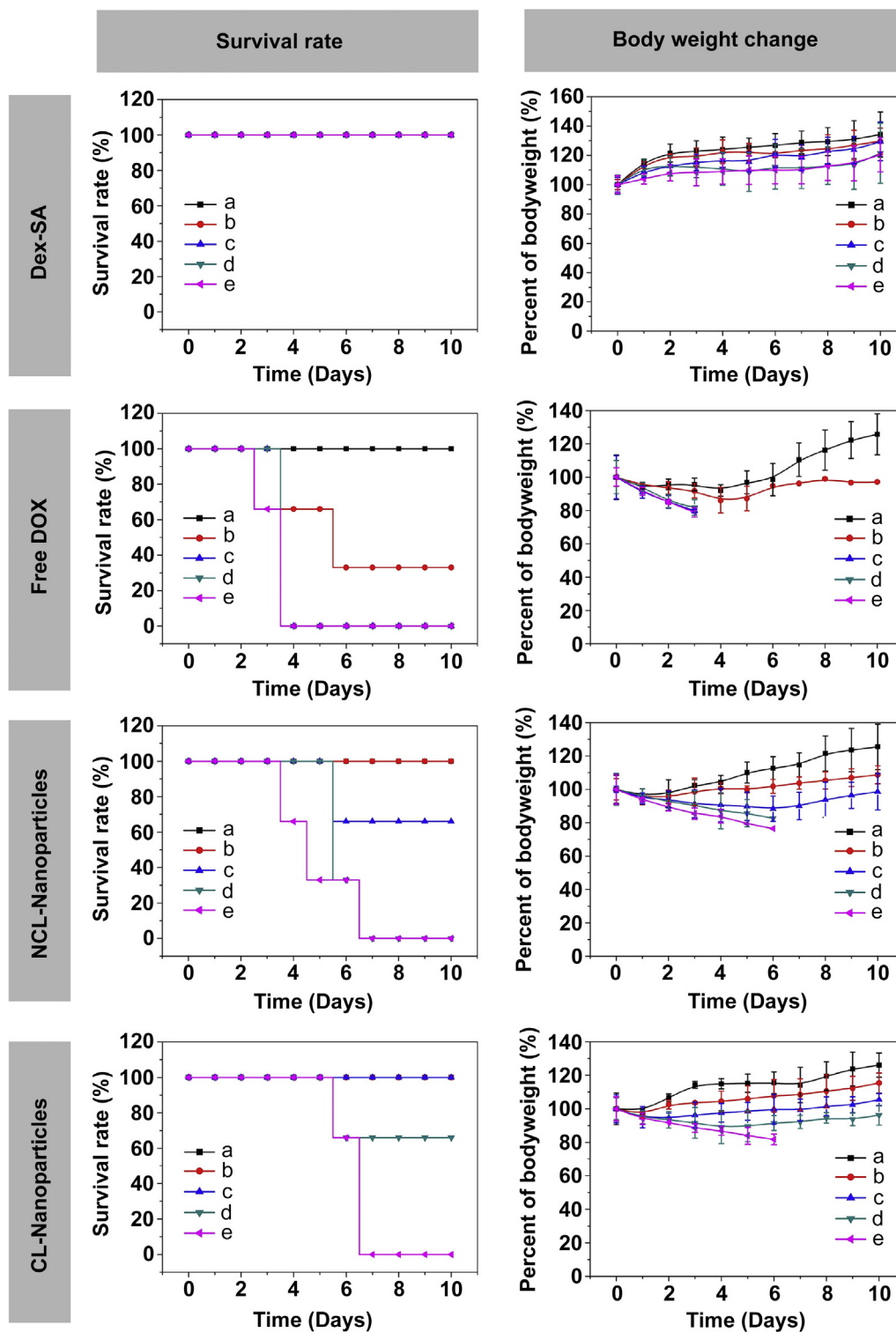


**Fig. 6.** Survival rate and body weight change of Kunming mice treated with Dex-SA at a dose of (a) 0, (b) 400, (c) 600, (d) 800 and (e) 1000 mg kg<sup>-1</sup>, free DOX, Dex-SA-DOX and Dex-SA-DOX-CISPLATIN at a dose of (a) 5, (b) 10, (c) 15, (d) 20 and (e) 25 mg kg<sup>-1</sup> DOX.

CISPLATIN), suggesting that the crosslinking procedure was critical for the enhanced antitumor activity. The enhanced tumor inhibition of the Dex-SA-DOX-CISPLATIN might be explained by the enhanced accumulation of the crosslinked nanoparticles at the tumor site. Furthermore, the effective encapsulation of DOX against leakage in the bloodstream and the facilitated intracellular release

of DOX might also contribute to the observed enhanced antitumor efficacy.

All the mice were alive during the experimental period. Dex-SA-DOX-CISPLATIN treatment resulted in almost no difference in the physical activity level and body weight after 18 days. However, a slight loss of body weight in mice receiving Dex-SA-DOX (3.2% body

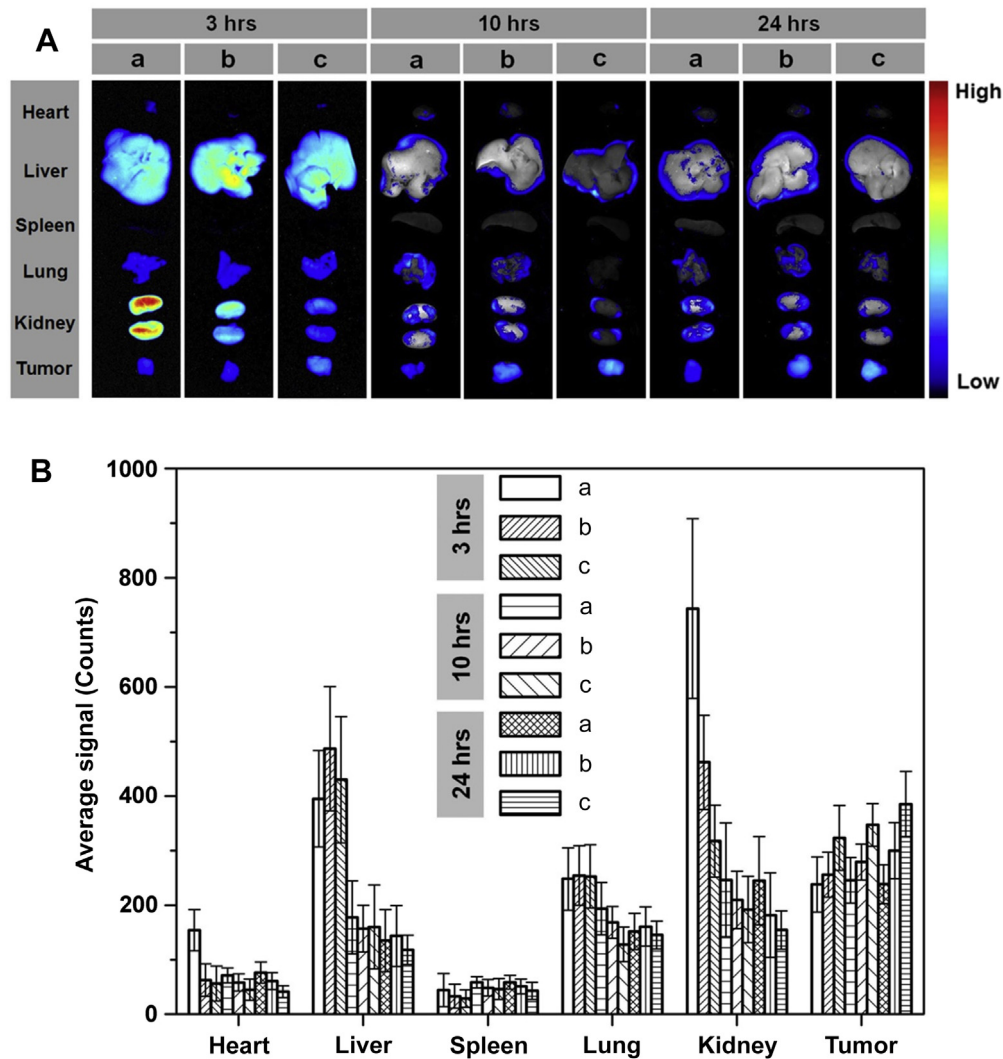


**Fig. 7.** (A) *Ex vivo* DOX fluorescence images showing the drug bio-distribution of (a) free DOX, (b) Dex-SA-DOX and (c) Dex-SA-DOX-CISPLATIN in nude mice bearing A549 tumor at 3, 10 and 24 h post-injection; (B) Average signals collected from the major organs (heart, liver, spleen, lung and kidney) and tumor in nude mice bearing A549 tumor after the treatment of (a) free DOX, (b) Dex-SA-DOX and (c) Dex-SA-DOX-CISPLATIN at different time points.

weight loss, Fig. 8B) and an obvious loss were noted in the free drug treatment groups (5.8 and 7.6% body weight loss for groups b and d, respectively), indicating that DOX became less toxic after micellization and crosslinking. These results were in accordance with the phenomena received from the tolerability study. Such differences demonstrated that the encapsulation of DOX in the reversible crosslinked nanoparticles reduced the random exposure of drug to normal tissues, increased the passive accumulation efficacy of the nanoparticles to the tumor sites, and thus led to lower undesirable systemic toxicities and enhanced antitumor efficacy.

### 3.10. Histological and immunohistochemical analyses

To further evaluate the antitumor efficacy after treatment with various formulations, the tumors and solid organs (heart, liver, spleen, lung and kidney) were dissected from mice and sectioned for pathology analysis.

As shown in Fig. 8C, the tumor cells with a large nucleus and a spherical or spindle shape were observed in the tumor tissue treated with PBS group, in which more chromatin and binucleolates were also observed, indicating a rapid tumor growth. In contrast,

the tumor cellularity, as evaluated by average tumor cell numbers of each microscopic field [55], decreased significantly and various degree of tissue necrosis, extensive nuclear shrinkage and fragmentation were observed in the free DOX and the DOX-loaded formulations treated groups. Chromatin was concentrated and distributed around the edge, and nuclei became pyknotic, fragmented or absent, especially for the Dex-SA-DOX-CISPLATIN treated tumor cells. The necrosis area in the Dex-SA-DOX-CISPLATIN group was the largest among the tested groups, while the free DOX and Dex-SA-DOX groups displayed a relatively lower necrotic level.

As shown by the TUNEL assay, tumors treated with all the DOX formulations had extensive regions of apoptotic cells, especially for the Dex-SA-DOX-CISPLATIN administered tumors, whereas such apoptotic cells were much less present in the tumors treated with PBS and low dose of cisplatin (free cisplatin and Dex-SA-CISPLATIN), consistent with the *in vivo* antitumor capability and H&E stain results. To further confirm the tumor apoptosis, the cleaved 25 kDa fragment of PARP1, one of the essential substrates cleaved by both caspase-3 and -7 [30,56], was analyzed in the tumor sections by immunohistochemistry. Intensive positive signals

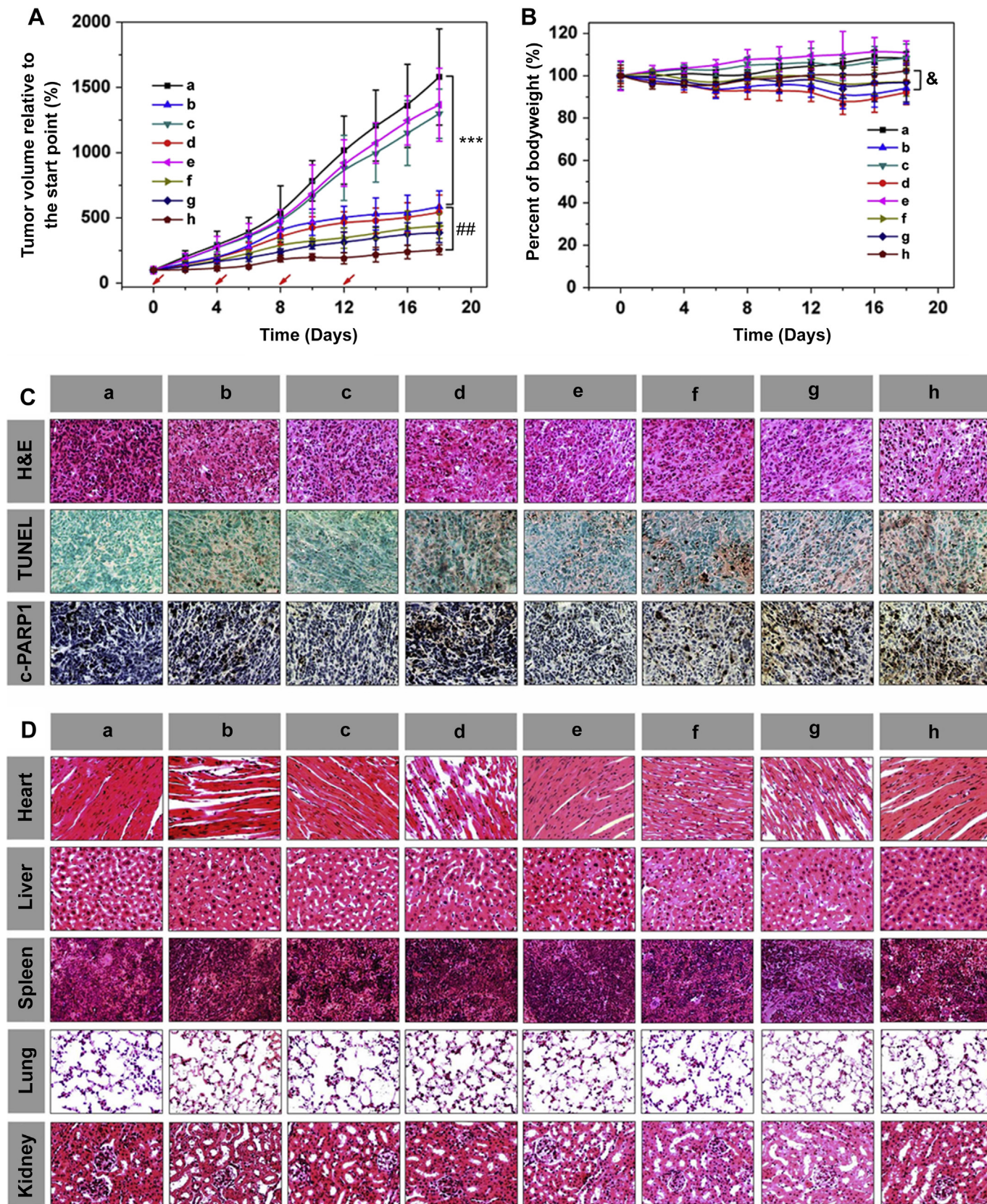


**Fig. 8.** *In vivo* antitumor efficacy and histological observation of major organs of (a) PBS, (b) free DOX ( $3.0 \text{ mg kg}^{-1}$ ), (c) free cisplatin ( $0.32 \text{ mg kg}^{-1}$ ), (d) free DOX ( $3 \text{ mg kg}^{-1}$ ) plus free cisplatin ( $0.32 \text{ mg kg}^{-1}$ ), (e) Dex-SA-CISPLATIN ( $0.32 \text{ mg kg}^{-1}$  cisplatin eq.), (f) Dex-SA-DOX ( $3.0 \text{ mg kg}^{-1}$ ), (g) Dex-SA-DOX ( $3.0 \text{ mg kg}^{-1}$ ) plus Dex-SA-CISPLATIN ( $0.32 \text{ mg kg}^{-1}$  cisplatin eq.) and (h) Dex-SA-DOX-CISPLATIN ( $3.0 \text{ mg kg}^{-1}$  DOX eq.) in the A549 tumor bearing mouse model. (A) Tumor sizes of the mice as a function of time. The arrows represent the day on which the intravenous tail vein injection was performed; (B) Body weight changes with the time of tumor-bearing mice; (C) *Ex vivo* histological, TUNEL and immunohistochemical analyses of A549 tumor sections (18 days after the first treatment). Nuclei were stained bluish violet, whereas extracellular matrix and cytoplasm were stained pink in H&E staining. Brown and green stains indicated apoptotic and normal cells, respectively, in TUNEL analysis; brown and blue stains indicated cleaved PARP and nuclei, respectively, in immunohistochemical assay; (D) Histologic assessments of major organs with H&E staining in mice. (For interpretation of the references to color in this figure legend, the reader is referred to the web version of this article.)

increased in the Dex-SA-DOX-CISPLATIN treated tumors compared with free DOX and Dex-SA-DOX treated ones, indicating that more cells underwent apoptosis in these groups. Our results demonstrated that Dex-SA-DOX-CISPLATIN could efficiently deliver DOX to the NSCLC tumor, leading to reduced cell proliferation and increased apoptosis *in vivo*, which resulted in a persistent inhibition of tumor growth.

Long-term toxicity is a major concern for *in vivo* applications of chemotherapy. Representative sections of several susceptible organs including heart, liver, spleen, lung and kidney taken at day 6 after the last injections from control mice receiving PBS and mice receiving various drug formulations were harvested and stained by H&E (Fig. 8D). Histological analysis of fixed tissues showed that no significant morphological changes could be detected in spleen and lung derived from animals in the control group compared to mice treated with free DOX, Dex-SA-DOX and Dex-SA-DOX-CISPLATIN. However, compared with the PBS control group, varying degree of organ damages of the treatment groups, including heart, liver, and kidney, were observed. Free DOX treated groups (group b and d) displayed noticeable signals of damage in heart, with the critical pathological changes and necrosis of the muscle fibers in cardiac tissues. In contrast, treatment of the tumor-bearing mice by DOX-incorporated nanoparticles, especially the crosslinked formulation obviously reduced the blight of heart. Slight structural disturbance with increased necrosis of hepatocytes could be observed in liver for free DOX treated group, but the degree was more moderate than the Dex-SA-DOX treated group. This was in accordance with the results of biodistribution study (Fig. 7), in which the accumulation of the NCL-Nanoparticles in liver was found relatively high due to their highly negatively charged surfaces. However, after the *in situ* crosslinking by cisplatin, the side effects were distinctly inhibited (Dex-SA-DOX-CISPLATIN, group h). It's worth noting that free cisplatin at a low dose (group c and d) could also induce severe nephrotoxicity (e.g., marked necrosis in proximal tubules, increased vacuole formation in proximal tubules, thickening of the mesangium and glomerular basement membrane, and contraction of epithelial luminal space). Whereas, the nephrotoxicity of cisplatin could be significantly inhibited after chelation (group e and h), suggesting that Dex-SA-DOX-CISPLATIN could allow the long-term administration.

#### 4. Conclusions

We have demonstrated that DOX-loaded, dextran-based reversible crosslinked micellar nanoparticles can efficiently deliver DOX into cancer cells *in vitro*, and reduce A549 xenograft tumor size *in vivo*. Importantly, *in situ* crosslinking of the DOX-loaded polysaccharide nanoparticles by introducing a small amount of cisplatin as the crosslinker, could significantly increase the surface charge and stability, which would further improve the tolerability, *in vivo* pharmacokinetics, biodistribution, and antitumor efficacy, and reduce drug-related multiorgan toxicity side-effect. Furthermore, systemic delivery of the crosslinked nanoparticles carrying DOX *via* intravenous injection could significantly inhibit tumor growth in A549 xenograft murine model due to its prolonged blood circulation, enhanced drug accumulation and facilitated intracellular release in the tumor cells. The current study also demonstrated that pH responsive polysaccharide-based cisplatin-crosslinked nanoparticles held great potential for achieving an optimal therapeutic effect of the transported drugs in cancer therapy. This design could be extended to nanoparticle delivery systems for a broad range of cationic drugs. A more comprehensive study of such nanoparticle systems is in progress to gain a better understanding of the efficacy of such systems in metastatic breast carcinoma and primary colon cancer.

#### Acknowledgments

This research was financially supported by National Natural Science Foundation of China (Projects 51173184, 51373168, 51273169, 21104076, 51233004 and 51021003), Ministry of Science and Technology of China (International Cooperation and Communication Program 2011DFR51090) and Program of Scientific Development of Jilin Province in China (20130727050YY and 20130206066GX).

#### References

- [1] Ta HT, Dass CR, Larson I, Choong PFM, Dunstan DE. A chitosan-dipotassium orthophosphate hydrogel for the delivery of doxorubicin in the treatment of osteosarcoma. *Biomaterials* 2009;30:3605–13.
- [2] Xu W, Siddiqui IA, Nihal M, Pilla S, Rosenthal K, Mukhtar H, et al. Aptamer-conjugated and doxorubicin-loaded unimolecular micelles for targeted therapy of prostate cancer. *Biomaterials* 2013;34:5244–53.
- [3] Long CY, Sheng MM, He B, Wu Y, Wang G, Gu ZW. Comparison of drug delivery properties of PEG-b-pdhpcc micelles with different compositions. *Chin J Polym Sci* 2012;30:387–96.
- [4] Xu X, Li Y, Li H, Liu R, Sheng M, He B, et al. Smart nanovehicles based on pH-triggered disassembly of supramolecular peptide-amphiphiles for efficient intracellular drug delivery. *Small* 2013. <http://dx.doi.org/10.1002/sml.201301885>.
- [5] Kuang Y, Liu J, Liu Z, Zhuo R. Cholesterol-based anionic long-circulating cisplatin liposomes with reduced renal toxicity. *Biomaterials* 2012;33:1596–606.
- [6] Xiao HH, Song HQ, Yang Q, Cai HD, Qi RG, Yan LS, et al. A prodrug strategy to deliver cisplatin(IV) and paclitaxel in nanomicelles to improve efficacy and tolerance. *Biomaterials* 2012;33:6507–19.
- [7] Lee SM, O'Halloran TV, Nguyen ST. Polymer-caged nanobins for synergistic cisplatin-doxorubicin combination chemotherapy. *J Am Chem Soc* 2010;132:17130–8.
- [8] Yang CA, Tan JPK, Cheng W, Attia ABE, Ting CTY, Nelson A, et al. Supramolecular nanostructures designed for high cargo loading capacity and kinetic stability. *Nano Today* 2010;5:515–23.
- [9] Ebrahim Attia AB, Yang C, Tan JP, Gao S, Williams DF, Hedrick JL, et al. The effect of kinetic stability on biodistribution and anti-tumor efficacy of drug-loaded biodegradable polymeric micelles. *Biomaterials* 2013;34:3132–40.
- [10] Ke X-Y, Lin Ng VW, Gao S-J, Tong YW, Hedrick JL, Yang YY. Co-delivery of thioridazine and doxorubicin using polymeric micelles for targeting both cancer cells and cancer stem cells. *Biomaterials* 2014;35:1096–108.
- [11] Song W, Li M, Tang Z, Li Q, Yang Y, Liu H, et al. Methoxypoly(ethylene glycol)-block-poly(L-glutamic acid)-loaded cisplatin and a combination with iRGD for the treatment of non-small-cell lung cancers. *Macromol Biosci* 2012;12:1514–23.
- [12] Li M, Song W, Tang Z, Lv S, Lin L, Sun H, et al. Nanoscaled poly(L-glutamic acid)/doxorubicin-amphiphile complex as pH-responsive drug delivery system for effective treatment of nonsmall cell lung cancer. *ACS Appl Mater Interfaces* 2013;5:1781–92.
- [13] Li M, Lv S, Tang Z, Song W, Yu H, Sun H, et al. Polypeptide/doxorubicin hydrochloride polymersomes prepared through organic solvent-free technique as a smart drug delivery platform. *Macromol Biosci* 2013;13:1150–62.
- [14] Ding J, Xiao C, Li Y, Cheng Y, Wang N, He C, et al. Efficacious hepatoma-targeted nanomedicine self-assembled from galactopeptide and doxorubicin driven by two-stage physical interactions. *J Control Release* 2013;169:193–203.
- [15] Wu Y, Chen W, Meng F, Wang Z, Cheng R, Deng C, et al. Core-crosslinked pH-sensitive degradable micelles: a promising approach to resolve the extracellular stability versus intracellular drug release dilemma. *J Control Release* 2012;164:338–45.
- [16] Dai J, Lin S, Cheng D, Zou S, Shuai X. Interlayer-crosslinked micelle with partially hydrated core showing reduction and pH dual sensitivity for pin-pointed intracellular drug release. *Angew Chem Int Ed* 2011;50:9404–8.
- [17] Chen W, Cheng Y, Wang B. Dual-responsive boronate crosslinked micelles for targeted drug delivery. *Angew Chem Int Ed* 2012;51:5293–5.
- [18] Klinger D, Landfester K. Enzymatic- and light-degradable hybrid nanogels: crosslinking of polyacrylamide with acrylate-functionalized dextrans containing photocleavable linkers. *J Polym Sci Part A Polym Chem* 2012;50:1062–75.
- [19] Xiong MH, Li YJ, Bao Y, Yang XZ, Hu B, Wang J. Bacteria-responsive multifunctional nanogel for targeted antibiotic delivery. *Adv Mater* 2012;24:6175–80.
- [20] Xiong MH, Bao Y, Yang XZ, Wang YC, Sun B, Wang J. Lipase-sensitive polymeric triple-layered nanogel for "on-demand" drug delivery. *J Am Chem Soc* 2012;134:4355–62.
- [21] Jia Y, Fei J, Cui Y, Yang Y, Gao L, Li J. pH-responsive polysaccharide microcapsules through covalent bonding assembly. *Chem Commun* 2011;47:1175–7.
- [22] Li Y-L, Zhu L, Liu Z, Cheng R, Meng F, Cui J-H, et al. Reversibly stabilized multifunctional dextran nanoparticles efficiently deliver doxorubicin into the nuclei of cancer cells. *Angew Chem Int Ed* 2009;48:9914–8.

- [23] Rijcken CJ, Snel CJ, Schiffflers RM, van Nostrum CF, Hennink WE. Hydrolysable core-crosslinked thermosensitive polymeric micelles: synthesis, characterisation and *in vivo* studies. *Biomaterials* 2007;28:5581–93.
- [24] Li MQ, Tang ZH, Sun H, Ding JX, Song WT, Chen XS. pH and reduction dual-responsive nanogel cross-linked by quaternization reaction for enhanced cellular internalization and intracellular drug delivery. *Polym Chem* 2013;4:1199–207.
- [25] Bahadur KCR, Thapa B, Xu P. pH and redox dual responsive nanoparticle for nuclear targeted drug delivery. *Mol Pharm* 2012;9:2719–29.
- [26] Shi F, Ding J, Xiao C, Zhuang X, He C, Chen L, et al. Intracellular microenvironment responsive PEGylated polypeptide nanogels with ionizable cores for efficient doxorubicin loading and triggered release. *J Mater Chem* 2012;22:14168–79.
- [27] Cho H-J, Yoon I-S, Yoon HY, Koo H, Jin Y-J, Ko S-H, et al. Polyethylene glycol-conjugated hyaluronic acid-ceramide self-assembled nanoparticles for targeted delivery of doxorubicin. *Biomaterials* 2012;33:1190–200.
- [28] Zhu S, Hong M, Tang G, Qian L, Lin J, Jiang Y, et al. Partly PEGylated poly-amidoamine dendrimer for tumor-selective targeting of doxorubicin: the effects of PEGylation degree and drug conjugation style. *Biomaterials* 2010;31:1360–71.
- [29] Kato J, Li Y, Xiao K, Lee JS, Luo J, Tuscano JM, et al. Disulfide cross-linked micelles for the targeted delivery of vincristine to B-cell lymphoma. *Mol Pharm* 2012;9:1727–35.
- [30] Fu C, Lin L, Shi H, Zheng D, Wang W, Gao S, et al. Hydrophobic poly (amino acid) modified PEI mediated delivery of rev-casp-3 for cancer therapy. *Biomaterials* 2012;33:4589–96.
- [31] Wong HL, Bendayan R, Rauth AM, Li Y, Wu XY. Chemotherapy with anticancer drugs encapsulated in solid lipid nanoparticles. *Adv Drug Deliv Rev* 2007;59:491–504.
- [32] Ding JX, Shi FH, Xiao CS, Lin L, Chen L, He CL, et al. One-step preparation of reduction-responsive poly(ethylene glycol)-poly (amino acid)s nanogels as efficient intracellular drug delivery platforms. *Polym Chem* 2011;2:2857–64.
- [33] Khlebtsov BN, Khlebtsov NG. On the measurement of gold nanoparticle sizes by the dynamic light scattering method. *Colloid J* 2011;73:118–27.
- [34] Wang Z, Yu Y, Dai W, Lu J, Cui J, Wu H, et al. The use of a tumor metastasis targeting peptide to deliver doxorubicin-containing liposomes to highly metastatic cancer. *Biomaterials* 2012;33:8451–60.
- [35] Xiao K, Li Y, Luo J, Lee JS, Xiao W, Gonik AM, et al. The effect of surface charge on *in vivo* biodistribution of PEG-oligocholeic acid based micellar nanoparticles. *Biomaterials* 2011;32:3435–46.
- [36] Ding M, Song N, He X, Li J, Zhou L, Tan H, et al. Toward the next-generation nanomedicines: design of multifunctional multiblock polyurethanes for effective cancer treatment. *ACS Nano* 2013;7:1918–28.
- [37] Huang W-C, Chiang W-H, Huang Y-F, Lin S-C, Shih Z-F, Chern C-S, et al. Nano-scaled pH-responsive polymeric vesicles for intracellular release of doxorubicin. *J Drug Target* 2011;19:944–53.
- [38] Sanson C, Schatz C, Le Meins JF, Soum A, Thevenot J, Garanger E, et al. A simple method to achieve high doxorubicin loading in biodegradable polymersomes. *J Control Release* 2010;147:428–35.
- [39] Dufort S, Sancey L, Coll J-L. Physico-chemical parameters that govern nanoparticles fate also dictate rules for their molecular evolution. *Adv Drug Deliv Rev* 2012;64:179–89.
- [40] Ren DM, Dalmau M, Randall A, Shindel MM, Baldi P, Wang SW. Biomimetic design of protein nanomaterials for hydrophobic molecular transport. *Adv Funct Mater* 2012;22:3170–80.
- [41] Pu Y, Chang S, Yuan H, Wang G, He B, Gu Z. The anti-tumor efficiency of poly(L-glutamic acid) dendrimers with polyhedral oligomeric silsesquioxane cores. *Biomaterials* 2013;34:3658–66.
- [42] Zhou K, Wang Y, Huang X, Luby-Phelps K, Sumer BD, Gao J. Tunable, ultra-sensitive pH-responsive nanoparticles targeting specific endocytic organelles in living cells. *Angew Chem Int Ed* 2011;50:6109–14.
- [43] Wei R, Cheng L, Zheng M, Cheng R, Meng F, Deng C, et al. Reduction-responsive disassemblable core-cross-linked micelles based on poly (ethylene glycol)-b-poly (n-2-hydroxypropyl methacrylamide)-lipoic acid conjugates for triggered intracellular anticancer drug release. *Biomacromolecules* 2012;13:2429–38.
- [44] Sun Y, Zou W, Bian S, Huang Y, Tan Y, Liang J, et al. Bioreducible PAA-g-PEG graft micelles with high doxorubicin loading for targeted antitumor effect against mouse breast carcinoma. *Biomaterials* 2013;34:6818–28.
- [45] Ganta S, Devalapally H, Shahiwal A, Amiji M. A review of stimuli-responsive nanocarriers for drug and gene delivery. *J Control Release* 2008;126:187–204.
- [46] Zhao L, Ding JX, Xiao CS, He P, Tang ZH, Pang X, et al. Glucose-sensitive polypeptide micelles for self-regulated insulin release at physiological pH. *J Mater Chem* 2012;22:12319–28.
- [47] Yue J, Wang R, Liu S, Wu SH, Xie ZG, Huang YB, et al. Reduction-responsive shell-crosslinked micelles prepared from Y-shaped amphiphilic block copolymers as a drug carrier. *Soft Matter* 2012;8:7426–35.
- [48] Talelli M, Morita K, Rijcken CJF, Aben RWM, Lammers T, Scheeren HW, et al. Synthesis and characterization of biodegradable and thermosensitive polymeric micelles with covalently bound doxorubicin-glucuronide prodrug via click chemistry. *Bioconjug Chem* 2011;22:2519–30.
- [49] Jin EL, Zhang B, Sun XR, Zhou ZX, Ma XP, Sun QH, et al. Acid-active cell-penetrating peptides for *in vivo* tumor-targeted drug delivery. *J Am Chem Soc* 2013;135:933–40.
- [50] Li SD, Howell SB. CD44-Targeted microparticles for delivery of cisplatin to peritoneal metastases. *Mol Pharm* 2010;7:280–90.
- [51] Št'astný M, Plocová D, Etrych T, Ulbrich K, Říhová B. HPMA-hydrogels result in prolonged delivery of anticancer drugs and are a promising tool for the treatment of sensitive and multidrug resistant leukaemia. *Eur J Cancer* 2002;38:602–8.
- [52] Ma PA, Liu S, Huang YB, Chen XS, Zhang LP, Jing XB. Lactose mediated liver-targeting effect observed by *ex vivo* imaging technology. *Biomaterials* 2010;31:2646–54.
- [53] Lee SY, Kim S, Tyler JY, Park K, Cheng JX. Blood-stable, tumor-adaptable disulfide bonded mPEG-(Cys)(4)-PDLLA micelles for chemotherapy. *Biomaterials* 2013;34:552–61.
- [54] Lee AL, Venkataraman S, Sirat SB, Gao S, Hedrick JL, Yang YY. The use of cholesterol-containing biodegradable block copolymers to exploit hydrophobic interactions for the delivery of anticancer drugs. *Biomaterials* 2012;33:1921–8.
- [55] Wang J, Sun X, Mao W, Sun W, Tang J, Sui M, et al. Tumor redox heterogeneity-responsive prodrug nanocapsules for cancer chemotherapy. *Adv Mater* 2013;25:3670–6.
- [56] Virág L, Robaszkiewicz A, Rodriguez-Vargas JM, Oliver FJ. Poly(ADP-ribose) signaling in cell death. *Mol Aspects Med* 2013;34:1153–67.